JES Focus Issue Honoring Allen J. Bard

Transient Interactions of Agglomerates of Sensitized TiO_2 Nanoparticles in Colloidal Suspensions

Ashantha Fernando, Pushpa Chhetri,* Krishna K. Barakoti,* Suman Parajuli, Rezvan Kazemi, and Mario A. Alpuche-Aviles,z**

Department of Chemistry, University of Nevada, Reno, Nevada 89557, USA

We present the study of dye-sensitized nanoparticles and their agglomerates with stochastic electrochemistry. We use a fluorine doped tin oxide (FTO) ultramicroelectrode (UME) with diameter in the range of 40 to 80 micrometers. To prepare the UME a sheet of perfluoroalkoxy alkane (PFA) is perforated to produce a recessed micro disk of the transparent conductive oxide. We demonstrate that the detection of the colloidal nanoparticles (NPs) sensitized with N719 is achieved via the interactions between agglomerates of the NPs that collide with the FTO. The NPs photooxidize MeOH and we detect the charge transfer from the NPs to the FTO ultramicroelectrode. The interactions between the dye sensitized NPs and the FTO yields oscillations that increase with exposure time. This increment in oscillation amplitude is assigned to changes in the aggregation of the NPs during the illumination even in the presence of 0.1 M supporting electrolyte. The formation of agglomerates is verified by dynamic light scattering and indicates that the agglomerates are able to separate photo-generated electrons and inject the carriers to the UME.
 [DOI: 10.1149/2.0041604jes] All rights reserved.

Manuscript submitted September 30, 2015; revised manuscript received November 11, 2015. Published December 3, 2015. *This paper is part of the JES Focus Issue Honoring Allen J. Bard.*

We present the study of dye-sensitized nanoparticles (DSNPs) and their agglomerates with stochastic electrochemistry. The field of stochastic electrochemistry for the detection of nanoparticles (NPs) has rapidly gained attention since the initial experiments proposed for the amperometric detection of electrocatalytic NPs by the Bard group[1–3] and others.[4–7] The stochastic studies have rapidly expanded to include contact,[2,3,8] i.e., irreversible interactions between NPs and the non-contact (reversible)[9,10] interactions between electrodes and NPs of metals. Electrochemical studies of discrete interactions in the "nano-impact" method by Compton[11–16] and co-workers include the complete electrolysis of NPs.[17] Single NP detection takes advantage of an electrocatalytic cycle that occurs at the NPs with catalytic NPs interacting with a mostly inert substrate. This enables a large signal amplification that has allowed the trapping and studying of single metal NPs.[18,19] Here, we use an analogous amplification and catalytic cycle that is driven by the interaction of photons with dye-sensitized NP in a colloidal suspension.

The use of dyes to modify NPs has been of broad scientific interest since the introduction of nanostructured dye sensitized solar cells (DSSCs) by O'Regan and Gratzel[20] in 1991 sparked interest in the use of nanoparticle films for solar energy conversion. Since then, a large effort has been devoted to improve the efficiency of these devices to meet current energy demand. The study of these events for films or NP ensembles are complicated by electron diffusion within the assembly and mass transport to and within the porous structures.[21] Therefore, we are developing the electrochemistry of colloidal semiconductors (SC) to study the electron transfer without complications of transport in and out of the film. This paper describes the detection of collisions of bare TiO_2 NPs sensitized with a commonly used dye (N719) at fluorine doped tin oxide (FTO) working electrode by photoelectrochemical current oscillations. Therefore, we propose that electrochemical studies of colloidal DSNPs will yield insight into the electron transfer events that happen at the SC/dye/electrolyte interface and carrier losses due to recombination. Our previous report demonstrated the stochastic detection of bare TiO_2 on Pt electrodes[22] but here we demonstrate the detection of dye sensitized NPs on FTO which yield electrochemical oscillations. We note previously reported studies of TiO_2 "slurries" and colloids[23–27] but our main goal is to be able to resolve the particle by particle contribution to obtain information that is not available from other ensemble studies in films or suspensions.

The proposed detection scheme is schematically presented in Figure 1 and is based on the widely accepted mechanism of charge separation in the dye sensitized solar cells. For simplicity, we are not showing the electron transfer step between the oxidized dye that in turn oxidizes the solvent, MeOH. The bandgap energy of TiO_2 anatase is 3.2 eV and thus it absorbs light with $\lambda < 388$ nm. In order to extend the light absorption into the visible region, dye molecules which absorb light in visible spectrum are usually anchored to the surface of these NPs.[20] When light interacts with these modified NPs, the dye absorbs light in the visible region of the spectrum, reaction (1) in Figure 1a; this populates the LUMO with electrons reaction (2). These electrons will be injected into the conduction band of the TiO_2 NP reaction (3) making them efficient light harvesters (see Figure 1a). When these DSNPs collide with positively biased FTO working electrode, the electrons in the conduction band will be transferred to the FTO and detected during the experiment.

Experimental

Reagents.— The electrolyte was tetrabutylammonium perchlorate (TBAP, ≥99.0%, Fluka) in acetonitrile (≥99.8%, Sigma-Aldrich), unless noted otherwise. Fluorine doped tin oxide coated glass slides (FTO Tec 8, Hartford Glass Co.), perfluoroalkoxy alkane sheets (PFA, nominal thickness, 0.001 inch or 25 μm thick, McMaster Carr), silver wires (1.0 mm in diameter, 99.999%, Alfa Aesar), Pt wires (0.5 mm and 0.1 mm in diameter, 99.95%, Alfa Aesar), were used for electrode preparation. Titanium(IV) isopropoxide, TTIP (97%), 2-propanol (≥99.8%), glacial acetic acid (≥99.7%) and spectrophotometric grade methanol (≥99.9%) were obtained from Sigma Aldrich. 18 MΩ cm water (Nanopure, Thermo Scientific) was used in all experiments. Alumina (MP Alumina N - Super 1, MP Biomedicals, Germany) was used in solvent purification. Di-tetrabutylammonium cis-bis(isothiocyanato)bis(2,2′-bipyridyl-4,4′-dicarboxylato)ruthenium(II), N719 was obtained from Sigma Aldrich and used as received.

Fabrication of FTO ultramicroelectrodes.— We prepared FTO ultramicroelectrodes in order to observe NP collisions. The main motivation for the preparation of UMEs is to increase the sensitivity of the measurement by reducing the background noise as the

*Electrochemical Society Student Member.
**Electrochemical Society Active Member.
zE-mail: malpuche@unr.edu

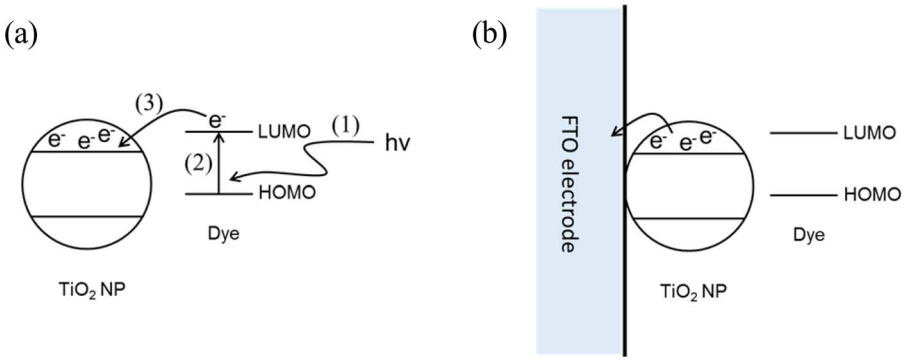

Figure 1. Schematics of the detection of DSNPs under illumination. a) Depicts light absorption and electron injection into the anchored NP by dye molecule. b) Describes the electron transfer from the DSNP interacting with FTO electrode.

photoelectrochemical (PEC) currents for these NPs are in the order of nano-amperes (nA). In the fabrication method, FTO plates were first cleaned with water and then with methanol and kept for 15 minutes immersed in the solvent in an ultrasonic bath. The cleaned FTO plates were then oven dried for 30 minutes at 120°C. A heated Pt wire (diam = 0.1 mm) previously fused to a borosilicate glass capillary was used to make pin holes on PFA sheets (thickness = 25 μm, area = 2.5 × 2.5 cm^2). A fire torch was used to heat the Pt wire. A homemade support was used to stretch the PFA sheets and a manual XY axes stage was used to hold the Pt wire fused capillary. The diameter of the holes made on the PFA sheets was comparable with that of the Pt wire being used. The smallest Pt diameter used to make pinholes was limited to 0.1 mm as the Pt wires with diam <0.1 mm were not strong enough to make pin holes. After perforating the PFA sheets they were cut into the size of the FTO plate (2.5 × 2.5 cm^2). The perforated PFA sheets were cleaned following the same procedure described above. The PFA sheets were then transferred to the dried FTO plates. To adhere the PFA to the FTO plates a few drops of MeOH were added onto the surface of the FTO plate. The as-prepared FTO plates were then baked at 350°C for 30 minutes with a ramping of 10°C/min in closed furnace. Optical micrographs were obtained for these FTO micro-electrodes using Leica DMI3000 B microscope equipped with a digital camera.

Preparation of TiO_2 NPs.— Anatase NPs were prepared by a modified procedure given of Zaban et al.[28] The details of our procedure are given elsewhere.[22] Briefly, NPs were prepared by hydrothermal growth from a mixture of 2-propanol (6.01 g) and TTIP (7.23 g) in glacial acetic acid (33.6 g) and de-ionized water (100 ml). The mixture was pre-concentrated for six hours on a heating plate kept at 80°C and transferred to an autoclave for hydrothermal growth at 230°C for 12 hours. The as-prepared TiO_2 NPs were extensively purified, first with deionized water and finally with spectrophotometric grade methanol (MeOH).

Preparation of dye sensitized TiO_2 NPs.— The dye sensitization of TiO_2 NPs was achieved by mixing a purified TiO_2 anatase colloidal suspension with N719 dye solution in EtOH.[29] A 10^3 higher concentration of the dye with respect to TiO_2 was preferred as one TiO_2 NP of 18 nm in diameter can accommodate ~600 dye molecules on its surface.[30] We performed the sensitization by mixing 2.27 × 10^{-4} M of dye molecules with 200 nM TiO_2 NPs in 20 mL of EtOH. After mixing, the sample was left undisturbed for one week in the dark. We note that for films in the dye solution, e.g., the procedure in Ref. 29, the sensitization of a TiO_2 NP film can be achieved by incubating TiO_2 film in a dye solution for 24 h in EtOH. However, for TiO_2 NPs suspended in MeOH we found that the time required for sensitization is much longer. The sensitized NPs were centrifuged to remove the excess dye molecules in the supernatant. The procedure for centrifugation in brief, 20 mL of the colloidal solution was transferred carefully into centrifuge tubes with 2 mL capacity. These were then centrifuged using a fixed angle centrifuge (AccuSpin Micro 17, Fisher Scientific) for 10 min at 13 000 rpm or 17 000 g. After the centrifugation, the supernatant was removed and the NPs were re-dispersed in spectrophotometric grade MeOH; using a sonicating bath. After sonication the samples were again centrifuged and this process was performed a total of 3 times. The final precipitate was used for the experiments after re-dispersing in a stock solution.

Photoelectrochemical measurements.— A specially designed electrochemical cell, with a working FTO ultramicroelectrode, platinum coil counter electrode (CE) and a home-made reference electrode (RE) containing 10 mM I^-/I_3^- and 0.1 M tetrabutylamoniumperchlorate (TBAP) in MeOH was used for PEC current measurements. All solutions were purged with argon for 20 minutes prior to every electrochemical measurement and sealed with a cap subsequently. Spectrophotometric grade MeOH containing 0.1 M TBAP was used as the blank unless otherwise stated. Samples were freshly prepared for each run by adding an aliquot of TiO_2 NPs or DSNPs to the blank solution to give a final NP concentration of 25 nM; the colloidal suspension was dispersed in an ultrasonic bath for at least 15 minutes prior to the PEC experiment. The applied potential was E_{app} = 0.32 V vs I^-/I_3^- (10 mM in MeOH) = 0.70 V vs NHE. For illumination, an ozone free Xe arc lamp (150 W) was used along with an IR water filter. A CHI 760 electrochemical station (CH Instruments) was used for all electrochemical measurements. Figure 2 is a schematic representation of the experimental setup. An automated shutter was used to control the illumination time of the samples and most of the time data were collected in the dark during the first 50 s.

Results and Discussion

Observation of photoelectrochemical (PEC) currents of DSNPs at FTO UMEs.— The size of the FTO UME is key to this experiment. By decreasing the diameter of the UME the background current decreases and this increases the signal to noise ratio for the small currents detected in the experiment (<100 nA). We make pin holes on PFA sheets by using 100 μm diameter Pt wires, the size of the FTO UMEs are in the range of 40 μm to 150 μm after baking. However, most of

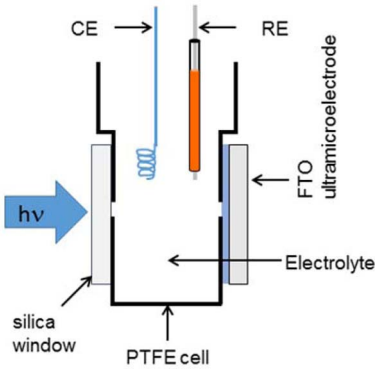

Figure 2. Schematic diagram of the experimental setup used in PEC current measurements.

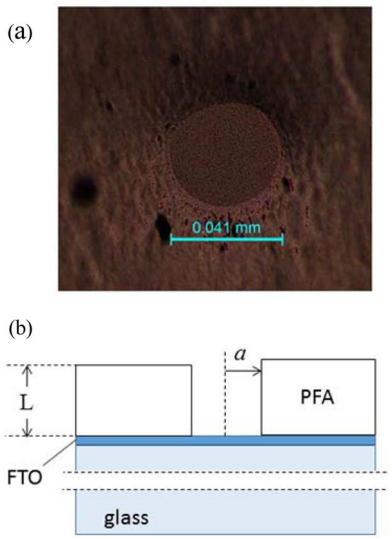

Figure 3. (a) Optical micrograph of FTO UME. (b) Schematics of the recessed disk.

them are below 100 μm in diameter. In our experiments we used FTO UMEs with diameters of 40 μm to 60 μm only. Figure 3 shows the optical micrograph obtained for one UME made in our lab.

The average diameter of the fabricated FTO UME was measured using the optical microscope and it came out to be ∼40 μm. We further studied the size and the behavior of the fabricated FTO UME using electrochemical methods. In this case we obtained cyclic voltammogram of ferrocene at FTO UME. A Ag wire and a Pt coil were used as reference and counter electrodes respectively. Ferrocene (0.78 mM) in MeOH with 0.15 M TBAP was used as the electrolyte. The solution was bubbled with Ar for 30 min and the cyclic voltammogram was obtained.

For a disk of radius a recessed in a cavity of depth L, the steady state current, $i_{s,r}$ is given by:[31]

$$i_{s,r} = 4nFDC^*a\left(\frac{1}{\frac{4L}{\pi a}+1}\right) \quad [1]$$

where n is the number of electrons in the redox process, F is the Faraday constant, D is the diffusion and C^* the concentration of the species. Equation 1 is the formula for the inlaid disk corrected with the factor $1/(4\ L/\pi a + 1)$ to account for the blocking effect of the 'barrier' around the disk. From the data in Figure 4, $i_{s,r} = 9.8$ nA, where $i_{s,r}$ is the diffusion limited current, n is the number of electrons transferred from the redox species, F is the faradaic constant, a is the radius and C^* the concentration. The thickness of the film L is shown in Figure 3b. For ferrocene $D_{Fc} = 1.7 \times 10^{-5}$ cm^2 s^{-1} and $n = 1$.[32] The concentration of ferrocene used was $C^* = 7.8 \times 10^{-7}$ mol cm^{-3}.

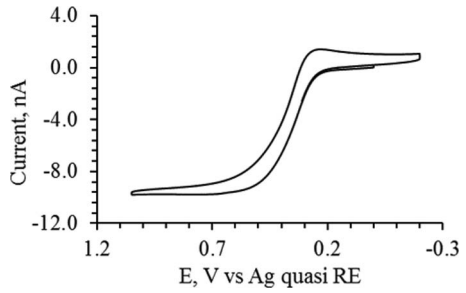

Figure 4. Cyclic voltammogram of a 40 μm diameter disk in 0.78 mM ferrocene in MeOH with 0.15 M TBAP under an Ar atmosphere. The scan rate (v) = 100 mV s^{-1}.

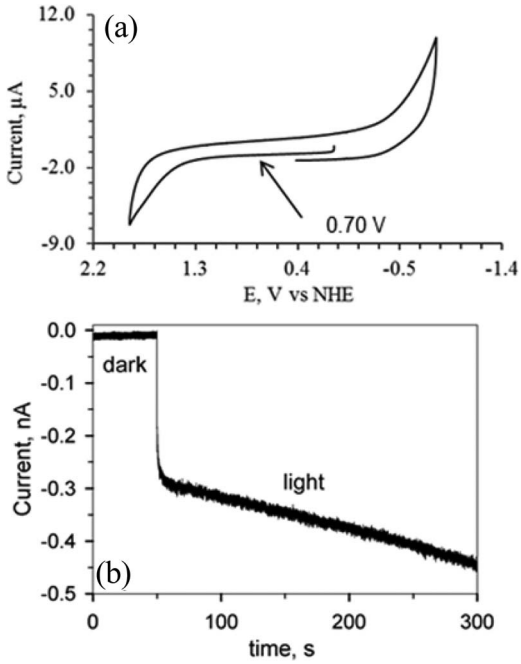

Figure 5. (a) Cyclic voltammogram of MeOH at FTO (diam = 0.7 cm) with 0.1 M $TBABF_4$. (b) Background current for a 50 μm diam UME at E_{app} = 0.7 V vs NHE. The electrolyte was purified with activated alumina and purged with Ar for 20 min.

The CV for the UME in Figure 4 fits the theory for a diameter of 40 μm and a film thickness of 2 μm around the recessed disk. This particular electrode was prepared by repeatedly heating the PFA film on the electrode and under these conditions the film is expected to melt and become thinner around the disk. We are currently optimizing the preparation of the micro disks of FTO and we will present our results elsewhere.[33] In this paper, we introduce the application of the FTO UME for the detection of transient interactions between agglomerates and the FTO. The use of UMEs minimizes the magnitude of the background faradaic and non-faradaic processes and this is essential to reduce the background noise to detect small currents <1 nA that originate from the suspended NPs and their agglomerates. A Faraday cage along with metal shields were used to reduce the background noise to <30 pA in the dark for the PEC measurement. We present a CV for a large FTO electrode (diam = 0.7 cm) in MeOH in Figure 5a to note that the use of FTO in MeOH affords a relatively large electrochemical window without observing the oxidation of MeOH. The oxidation at FTO appears at more positive potentials than E_{app} = 0.70 V vs NHE, which is the potential used for our measurements. The background current at potentials negative of −0.3 V vs NHE is due to faradaic processes in the FTO film. Therefore, this potential region was avoided during our experiments. The background of the UME for the MeOH blank with E_{app} = 0.70 V vs NHE is shown in Figure 5b. This is for an electrode with an area of 900 μm^2 (21 × 44 μm), and corresponds to the larger electrodes used in this work. Even for relatively large electrodes the current in the dark is less than 0.1 nA. Under illumination, the current is significantly higher, but it is <1 nA in the MeOH blank. This current continues to increase in the anodic direction probably due to residual photo-processes at the FTO electrode and the photooxidation of MeOH and impurities. However, in the time scale of an experiment the background is <1 nA. It is important that the background is minimized, due to the small amplitude of the current measurements in the collisions. In our current setup, we found that the exposed area of the electrode is the main limiting factor and we are working in optimizing the fabrication procedure to reduce the area of the FTO microelectrode. For the experiments presented here we only used electrodes that gave backgrounds of <1 nA in the MeOH solvent. Even though MeOH does

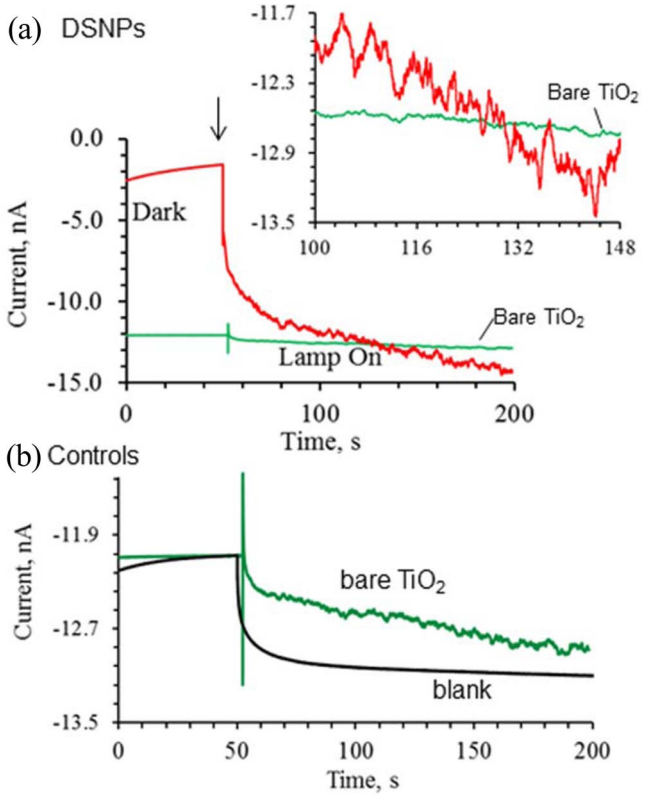

Figure 6. (a) Plot of current vs time for a suspension of 25 nM dye sensitized TiO_2 NPs (——, red) in MeOH containing 0.1 M TBAP at FTO UME. E_{app} = 0.70 V vs NHE illuminated with a Xe lamp. For comparison, the *i* vs *t* behavior of bare TiO_2 NPs in the same electrolyte and UME is also shown (——, green) with the same NP concentration of 25 nM (b) shows the same data in (a) for TiO_2 NPs compared with the electrolyte blank (——, black). Data were collected in the dark at the initial 50 s and then the electrolyte was illuminated with 150 W Xe arc lamp (marked with ↓).

not get oxidized at FTO at $E_{app} = 0.70$ V vs NHE, the current-vs-time graph shows a background current of −2.5 to −12 nA in the dark (see Figures 6a and 6b) with TiO_2 before illumination due to background processes in the FTO and trace impurities in the MeOH.

Collisions of dye sensitized NPs.— Current vs time curves were obtained for this and the results are shown in Figure 6. For comparison with of the dye-sensitized NPs (——, red) the data is plotted with the control of bare TiO_2 NPs (——, green) the responses obtained with TiO_2 NPs are plotted in the same graph and scale (a) with the inset showing a detail of the oscillations. The same data for bare TiO_2 NPs is also plotted in Figure 6b with the control experiment with the blank electrolyte (——, black). As expected, the current in the dark does not show the oscillations and only a monotonic current is observed (<30 pA) during the first 50 s of the data obtained. However, the sample with TiO_2 NPs clearly shows some oscillations that are not seen without NPs. When the system is illuminated with the 150 W Xe lamp (after 50 s, marked with ↓), a drift in current in the anodic direction can be seen which has a similar shape of what we observed with bare TiO_2 NPs interacting with FTO UMEs (Figure 6b). Upon illumination, colloids made of bare and modified NPs show a PEC current growing in the anodic direction (electrons transfer from the electrolyte/TiO_2 NPs to the FTO UME). After the initial transient that result from turning the illumination on, the oscillations due to DSNPs interacting with FTO ultra-microelectrode can be seen (e.g., Figure 6a and the inset). The observation of current oscillations instead of step wise behavior[2,8] is indicative of short term interaction between particles and the electrode. The DSNPs clearly show higher magnitude for the PEC current oscillations compared to bare TiO_2 NPs. N719

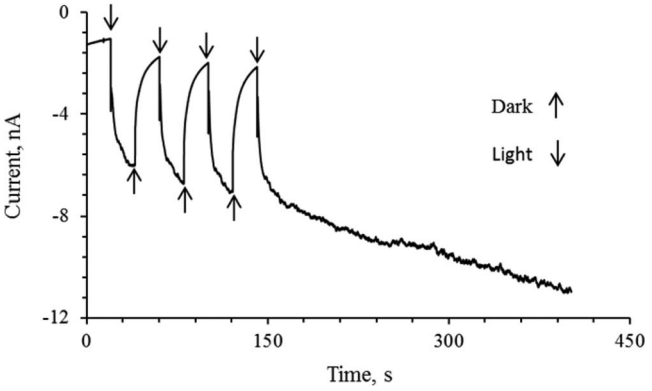

Figure 7. DSNPs suspension, 25 nM in MeOH with 0.1 M $TBABF_4$, saturated with Ar. Data were collected by chopping light on (↓) and off (↑) in 20 s intervals during the initial 150 s.

dye molecules harvest light efficiently in longer wavelengths (400 nm–700 nm) with respect to TiO_2 NPs, thus it provides more electrons in the conduction band of TiO_2. UV Visible spectra for the colloidal solutions of bare TiO_2 NPs and DSNPs in MeOH were obtained and they show similar spectra (not shown). The main reason for this is the larger absorption coefficient of TiO_2 NPs which is 4.3×10^8 $mol^{-1}cm^{-1}$ measured at 252 nm compared to that of N719 dye which is 13,900 $mol^{-1}cm^{-1}$ measured at 532 nm.[34] It is also noteworthy that in both the cases the initial value of current is not zero in the dark. This is likely due to the attachment of NPs onto the FTO UME which modifies the surface of the electrode. The magnitude of the initial drift in the current is a function of the number of NPs that interact with the surface of the working electrode. During the experiments with DSNPs, we observed aggregation of the NPs with time, i.e., it can be observed that large agglomerates of DSNPs, visible to the naked eye in the solution are formed during the course of the experiment with some of these large agglomerates precipitating after 20 min of light exposure. However, these sensitized NPs show reasonable stability under normal conditions: a suspension of dye-sensitized TiO_2 NPs was followed during 90 min in the UV Vis (Figure 8). Note that the absorbance of the solution is relatively constant which is consistent with the stability of the colloid in suspension without illumination. However, the observed changes in the colloidal stability under illumination are likely due to PEC process.

The relation of PEC current to the illumination was further studied. In this case, we chopped the light beam on (marked with ↓) and off (↑) for every 20 s. The data obtained are presented in Figure 7. We observe PEC current oscillations only under illumination and that there is a net anodic photocurrent probably due to dye adsorbed at the surface of the electrode and once the illumination is removed the current goes back to its background state. Overall, the photocurrent oscillations are

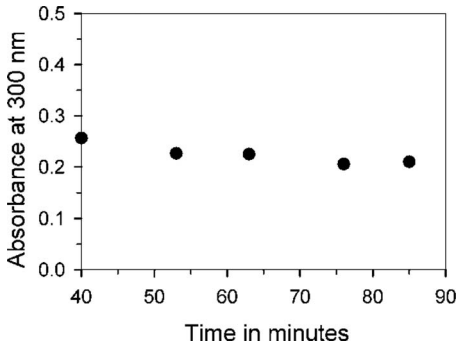

Figure 8. The absorbance vs time graph for 25 nM dye sensitized TiO_2 NPs suspended in MeOH with 0.1 M TBAP. The absorbance was recorded at 300 nm. A quartz cell with 1 mm path length was used.

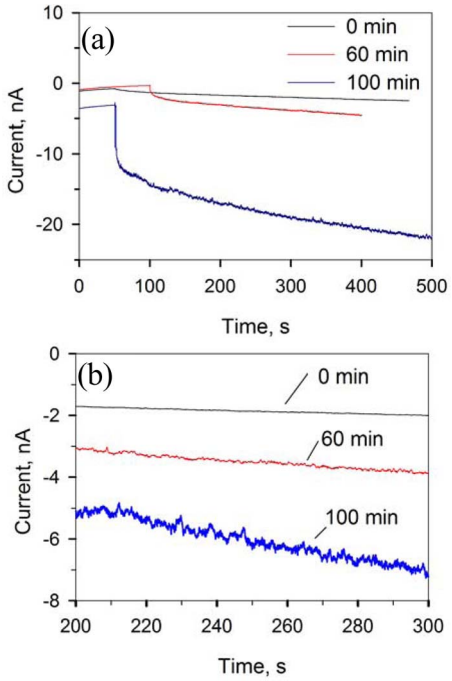

Figure 9. (a) Plot of current vs. time behavior for 25 nM DSNPs suspended in MeOH with 0.1 M TBAP. The data were collected over a period of time to study the effect of aggregations of NPs on PEC current transients. (b) Shows the data in (a) in detail.

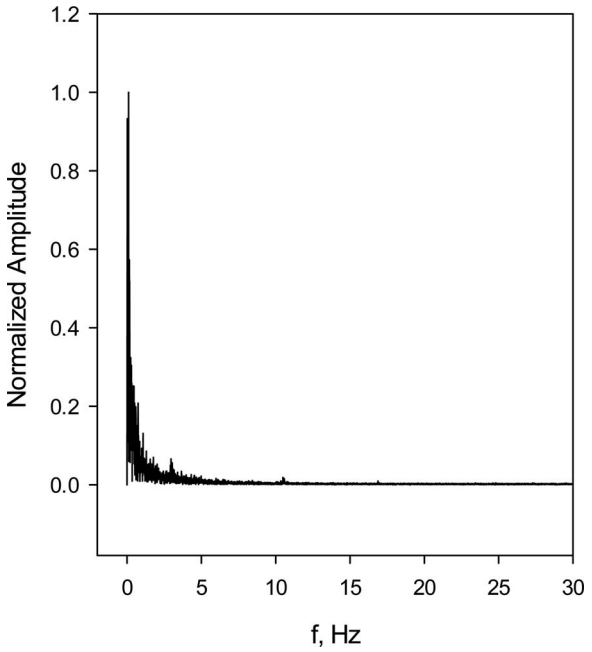

Figure 10. (a) Plot of the FFT analysis performed to the data in Figure 6a.

due to the photocatalytic process which is likely the photooxidation of MeOH to formaldehyde.

We further investigated the formation of agglomerates by performing a series of current vs time experiments in the same colloid after significantly different periods of illumination. An increase in the magnitude of PEC current oscillations with time was seen and the results are shown in Figure 9. The increase in the magnitude of the PEC oscillations can be related to the increase in the size of the agglomerates of colloids, both in the suspended solution and at the surface of the microelectrode. Note that the background level also increases with the illumination time, indicating that some of the DSNPs are stuck at the surface. However, we do not observe any discrete steps or individual blips. Overall, the data indicate that we are observing the superposition of several collisions within a short amount of time, with transients that have relatively large time scales, in the order of hundreds of milliseconds, as it will be described below.

As described previously, we observed the interaction of TiO_2 NPs with FTO UME as current oscillations in the current vs time curves. We concluded that these oscillations are due to agglomerates of TiO_2 NPs rather than due to single TiO_2 NPs as the charge transfer during the time of interaction cannot be explained by a single TiO_2 NP. The frequency of the collisions f_p is also a function of the electrode radius, r_d, (20 μm) and the diffusion coefficient of the NPs D_{NP} and C_{NP}^{bulk} is the NP concentration in MeOH. In order to accomplish this we can use the following relationship for the inlaid disk:[1,35]

$$f_p = 4D_{NP}r_dC_{NP}^{Bulk} \quad [2]$$

Similarly, the frequency of collision for the recessed disk, $f_{p,r}$ can be obtained by multiplying the overall flux by the area of the electrode:

$$f_{p,r} = 4D_{NP}r_dC_{NP}^{Bulk}\left(\frac{1}{\frac{4L}{\pi a}+1}\right) \quad [3]$$

Where all the symbols have the same meaning as above. This equation corresponds to the frequency of the inlaid disk, Eq. 2 multiplied by the conversion factor $1/(4\ L/\pi a + 1)$ in Equation 1. The correction factor for the mass transfer coefficient for the inlaid disk is small. For example, is ca. 0.4 for the nominal dimensions of the materials and electrodes used in this work, and will be within an order of magnitude for all our UMEs.

Based on the concentration of the NPs (25 nM) and assuming the diffusion coefficient to be 4.4×10^{-7} cm^2/s for an 18 nm diameter NP, we obtain a collision frequency of 5.3×10^4 Hz, which corresponds to tens of thousands of collisions per second. However, for the frequencies observed in our experiments the deviation is of several orders of magnitude with an experimental value of <15 Hz. We have performed fast Fourier transform (FFT) analysis of our experimental data and we have not been able to observe the expected high frequency components in the 10^3–10^4 Hz expected for the diffusion limited collision frequency given by Equations 2 and 3. For this analysis, the data was corrected for the background to analyze the oscillatory component of the signal. The FFT analysis of the data in Figure 6a is shown in Figure 10. As it can be seen in the figure, we were not able to observe the high frequency components that could be due to the collisions of individual NPs given by the diffusional flux. Further, most of the frequency components are around the 1 to 10 Hz, with the current method not being able to resolve the spectrum in the 1 Hz region.

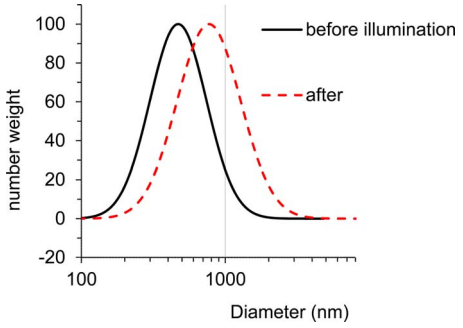

Figure 11. Dynamic light scattering data of a colloidal suspension of dye sensitized TiO_2 in MeOH, NP concentration of 25 nM in 0.1 M TBAP in MeOH. The data shows the size distribution before (——, black) and after (– – –, red) illumination for 20 min.

A final analysis was performed with the dynamic light scattering of the suspension under similar conditions to those in Figures 7 and 9: NP concentration of 25 nM in MeOH with the same electrolyte concentration, i.e., 0.1 M. The data show the colloidal size distribution before (——, black) and after illumination (– – –, red) for 20 min. We note that the dynamic light scattering data acquisition takes ca. 5 minutes and therefore, it is not possible to reproduce the exact time intervals depicted in Figure 9. Nevertheless, the dynamic light scattering data indicates that initially, the NPs are agglomerated with an average diameter of 520 nm and that after the illumination time, the size of the agglomerates increases significantly to an average diameter of 870 nm, consistent with the increase in amplitude observed in our collision experiments.

Instrumentation effects.— The resolution of a collision could be limited by the time response of the potentiostat. Similarly to the approach reported before for the occupancy of a particle[36] or a single molecule[37] at the electrode surface the response of our potentiostat to a particle arriving at the surface is considered in terms of the instrumental limitations. When a photoactive particle arrives at the inert electrode surface it requires a current step, i.e., an instantaneous change in current due to the particle contact. The potentiostat response can be modeled by the response in the rising part of the current:[38]

$$S(t) = k\left[1 - \exp\left(-\frac{2\pi}{\tau}t\right)\right] \quad [4]$$

Where $S(t)$ is the current output normalized to the new equilibrium value (i_f), t is the time and τ is the time constant of the circuit. The values of k and of τ depend on the operational amplifier circuit (e.g., on the feedback conditions and the open circuit gains of the amplifiers).[38] Conversely, the decay of the current when a particle leaves the surface will be:

$$S(t) = k\exp\left(-\frac{2\pi}{\tau}t\right) \quad [5]$$

To a first approximation, we assume $k = 1$ which makes the equation equivalent to a passive low-pass filter and we study the behavior of the circuit with the same gain used in our experiments. In these expressions, τ is defined as the reciprocal of the cutoff frequency of a low-pass filter, $f^0 = 1/\tau$. Figure 12 shows the test performed with our potentiostat to investigate the effect of the instrumentation on the time resolution of the current steps across a resistor. We have not attempted to reproduce exactly the conditions of our experimental particle collisions with an external circuit but rather, we investigate the time response of the potentiostat by applying a small potential step (0.05 V) to a 10 MΩ resistor with the sensitivity used in the amplifier for our experiments (1 nA/V). The figure shows the response to a potential step under the amplification gain used for our experiments. As it can be seen from the figure, the model in Eq. 4 gives a fair description of the current transient data observed with a $\tau = 12$ ms; for comparison the value of $\tau = 20$ ms is also shown to illustrate the sensitivity of the model and the instrument response to the τ value. Therefore, we will take the 12 ms as the response time constant of our instrument in the discussion of the time scale of our measurements.

Another issue to consider is the time delay that results from filtering the data. In the experiments presented here, a typical data interval is 16.4 ms, which corresponds to a sample frequency of 61 Hz, and this sets the internal filters of the potentiostat to a cut off frequency of $f = 150$ Hz (in the filtering frequency that the software selects automatically for the sampling rate and gain or "sensitivity"). The $f = 150$ Hz results in a time constant of ca. 20 ms, similar to that reported before.[36] However, the transients observed in the present work are in time scales that are larger than the limits of the time constant for the response or the signal filtering. The shape of a transient is shown in Figure 13 where the transient lasts over 300 ms. For comparison, the figure gives the theoretical occupancy, i.e., the response expected from a step based on the 12 ms time constant in Equations 4 and 5. The figure illustrates that the observed shape is not limited by the response

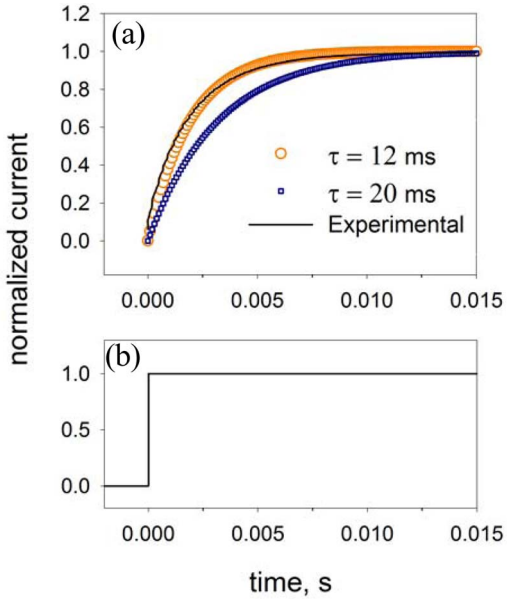

Figure 12. (a) Current transient from a potential step: (——) experimental results and the model applied to the transient, Eq. 4 with the best fit, (°, orange) $\tau = 12$ ms and (□, blue) $\tau = 20$ ms. (b) Theoretical response or "occupancy" resulting from the step. For the experimental data in (a) the potential step was 0.05 V across R = 10 MΩ with a final equilibrium current of 4.58 nA.

time of the potentiostat because the transient due to the potentiostat will be much faster as shown in Figure 13b. Note that the occupancy will be > 99% within 15 ms (Figure 12a). Further, a slower time constant, $\tau = 20$ ms is expected from the filtering frequency but this will make the rise and decay time of the signal ca. 20 ms, (cf. Figure 12a) which is much faster than the observed response in the order of hundreds of milliseconds. In summary, the observed shape is not due to the response time of the potentiostat or the signal filtering.

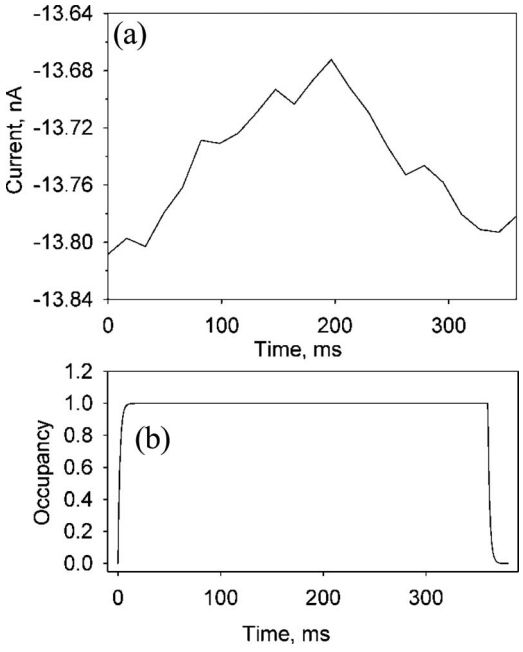

Figure 13. (a) Detail of a current transient and its comparison to the theoretical occupancy shown in (b) for a time constant, $\tau = 12$ ms of the instrumentation.

Table I. Diffusional properties and collision frequencies for the particles and agglomerates investigated.

Diameter, nm	D,[(a)] cm^2/s	τ_D,[(b)] μs	f_p,[(c)] s^{-1}	$f_{p,r}$,[(d)] s^{-1}
19	4.20×10^{-7}	0.024	50,623	20,249
520	1.54×10^{-8}	0.65	1,849	739
870	9.18×10^{-9}	1.10	1,105	442

[(a)]Diffusion coefficients calculated using the Stokes-Einstein equation.
[(b)]τ_D is the diffusional time scale for the particle to travel a distance l = 1 nm with $\tau = l^2/D$.
[(c)]Collision frequency calculated for an inlaid disk.
[(d)]Collision frequency calculated for a recessed disk used in this work. In the frequency calculation we use a concentration of 25 nM.

Diffusional time scales.— Table I shows that the NPs used in this work have diffusional time scales, τ_D, that are faster than the time constants due to filtering and that are intrinsic to the potentiostat speed. This is calculated based on the time it takes for a particle to travel a distance l = 1 nm to be within tunneling distance of the electrode. With $\tau_D = l^2/D$ we obtain diffusional time scales that are in the order of a microseconds even for the larger agglomerates observed in this work.

The frequencies of collision obtained with either Equation 4 or 5 yield frequencies of collision that are much higher, assuming a concentration of 25 nM, which corresponds to the upper limit of the collisions expected in the agglomeration process that we are studying here. In the formation of agglomerates one expects hundreds to thousands of discrete particles to make an 870 nm agglomerate, with a resulting lower concentration of agglomerates, and therefore, the frequency of 10^2 to 10^3 smaller, in line with the frequencies detected here. Finally, the frequency values calculated with Equations 4 or 5 do not take into account that a single NP or an agglomerate can undergo multiple collisions with the electrode[6] and therefore, the equation will correspond to the limit of the irreversible collisions for NPs.

Conclusions

We described a method to detect collisions of agglomerates of dye sensitized TiO_2 nanoparticles at working fluorine doped tin oxide ultramicroelectrode. A method was developed to fabricate FTO ultramicroelectrodes with diameter ranging from 40 – 80 μm. Mostly, the observed collisions of these particles suspended in methanol are photoelectrochemical current oscillations rather than steps or spikes. A growth in the magnitude of photoelectrochemical current with time was observed for the dye sensitized nanoparticles, with the magnitude of the photoelectrochemical oscillations being relatively small (<100 pA). We propose that the growth in photoelectrochemical current with time is due to the agglomeration of nanoparticles which is consistent with the low frequency observed in the electrochemical oscillations. The presence of agglomerates was confirmed by dynamic light scattering. The conditions for the experiment has to be further optimized in order to detect individual collisions of nanoparticles with spike like or step like current traces, as these provide important information about the mechanism and kinetics of the photoelectrochemical process. Overall, the data indicate that we are observing the superposition of several collisions within a short amount of time. Interestingly, our results suggest that the agglomerates are capable of performing electron transfer reactions despite the expected recombination losses. Besides our interest in isolating the electron transfer problem from the charge and transport in the agglomerate, current experiments are directed to understand the increase in agglomeration size with exposure to light. We note that the effect of agglomeration has been recently discussed in the electrochemistry of metal[15] and metal oxide NPs in magnetic fields,[16] and in FeO_x/Pt particles[39] but not we are not aware of other studies in the photocatalytic applications and therefore the aggregation and its implications in photocatalysis are the object of current investigation by our group.

Acknowledgments

This project was funded by NSF CHE-1255387 Career award and startup funds for Dr. Alpuche-Aviles from the University of Nevada, Reno.

References

1. X. Xiao and A. J. Bard, *J. Am. Chem. Soc.*, **129**(31), 9610 (2007).
2. X. Xiao, F.-R. F. Fan, J. Zhou, and A. J. Bard, *J. Am. Chem. Soc.*, **130**(31), 16669 (2008).
3. H. Zhou, F.-R. F. Fan, and A. J. Bard, *J. Phys. Chem. Lett.*, **1** (Copyright (C) 2012 American Chemical Society (ACS). All Rights Reserved.), 2671 (2010).
4. R. Dasari, K. Tai, D. A. Robinson, and K. J. Stevenson, *ACS Nano*, **8**(5), 4539 (2014).
5. R. Dasari, B. Walther, D. A. Robinson, and K. J. Stevenson, *Langmuir*, **29**(48), 15100 (2013).
6. M. Kang, D. Perry, Y.-R. Kim, A. W. Colburn, R. A. Lazenby, and P. R. Unwin, *J. Am. Chem. Soc.*, **137**(34), 10902 (2015).
7. S. E. F. Kleijn, B. Serrano-Bou, A. I. Yanson, and M. T. M. Koper, *Langmuir*, **29**(6), 2054 (2013).
8. A. J. Bard, H. Zhou, and S. J. Kwon, *Isr. J. Chem.*, **50** (Copyright (C) 2012 American Chemical Society (ACS). All Rights Reserved.), 267 (2010).
9. S. J. Kwon, F.-R. F. Fan, and A. J. Bard, *J. Am. Chem. Soc.*, **132**(38), 13165 (2010).
10. S. J. Kwon and A. J. Bard, *J. Am. Chem. Soc.*, **134**(16), 7102 (2012).
11. Y. Zhou, E. J. E. Stuart, J. Pillay, S. Vilakazi, R. Tshikhudo, N. V. Rees, and R. G. Compton, *Chem. Phys. Lett.*, **551**, 68 (2012).
12. S. V. Sokolov, C. Batchelor-McAuley, K. Tschulik, S. Fletcher, and R. G. Compton, *Chem. - Eur. J.*, **21**(30), 10741 (2015).
13. H. S. Toh, K. Jurkschat, and R. G. Compton, *Chem. - Eur. J.*, **21** 2998 (2015).
14. Y.-G. Zhou, N. V. Rees, and R. G. Compton, *Angew. Chem. Int. Ed.*, **50**(18), 4219 (2011).
15. S. V. Sokolov, K. Tschulik, C. Batchelor-McAuley, K. Jurkschat, and R. G. Compton, *Anal. Chem.*, **87**(19), 10033 (2015).
16. K. Tschulik and R. G. Compton, *Phys. Chem. Chem. Phys.*, **16**, 13909 (2014).
17. S. E. Ward Jones, F. W. Campbell, R. Baron, L. Xiao, and R. G. Compton, *J. Phys. Chem. C*, **112**(46), 17820 (2008).
18. J. Kim, B.-K. Kim, S. K. Cho, and A. J. Bard, *J. Am. Chem. Soc.*, **136**(23), 8173 (2014).
19. H. S. Ahn and A. J. Bard, *Angewandte Chemie*, **127**(46), 13957 (2015).
20. B. O'Regan and M. Gratzel, *Nature*, **353**(6346), 737 (1991).
21. B. Ohtani, *Journal of Photochemistry and Photobiology C: Photochemistry Reviews*, **11**(4), 157 (2010).
22. A. Fernando, S. Parajuli, and M. A. Alpuche-Aviles, *J. Am. Chem. Soc.*, **135**(30), 10894 (2013).
23. W. W. Dunn, Y. Aikawa, and A. J. Bard, *J. Electrochem. Soc.*, **128**(1), 222 (1981).
24. M. Graetzel and A. J. Frank, *J. Phys. Chem.*, **86**(15), 2964 (1982).
25. W. W. Dunn, Y. Aikawa, and A. J. Bard, *J. Am. Chem. Soc.*, **103**(12), 3456 (1981).
26. M. Gratzel, in *Electrochemistry in colloids and dispersions*, R. A. Mackay and J. Texter, eds., p. 357, VCH, New York, (1992).
27. H. Yoneyama, Y. Toyoguchi, and H. Tamura, *J. Phys. Chem.*, **76**(23), 3460 (1972).
28. A. Zaban, S. Ferrere, J. Sprague, and B. A. Gregg, *J. Phys. Chem. B*, **101**(1), 55 (1997).
29. B. Tan and Y. Wu, *J. Phys. Chem. B*, **110**(32), 15932 (2006).
30. B. C. O'Regan and J. R. Durrant, *Acc. Chem. Res.*, **42**(11), 1799 (2009).
31. A. M. Bond, D. Luscombe, K. B. Oldham, and C. G. Zoski, *J. Electroanal. Chem.*, **249**(1–2), 1 (1988).
32. A. J. Bard and L. R. Faulkner, *Electrochemical methods: fundamentals and applications*, p. 832, John Wiley & Sons, New York (2001).
33. P. Chhetri, G. Rana, R. Kazemi, and M. A. Alpuche-Aviles, *manuscript in preparation*, (2015).
34. Z.-S. Wang, H. Kawauchi, T. Kashima, and H. Arakawa, *Coord. Chem. Rev.*, **248**(13–14), 1381 (2004).
35. S. J. Kwon, H. Zhou, F.-R. F. Fan, V. Vorobyev, B. Zhang, and A. J. Bard, *Phys. Chem. Chem. Phys.*, **13**(12), 5394 (2011).
36. C.-H. Chen, E. R. Ravenhill, D. Momotenko, Y.-R. Kim, S. C. S. Lai, and P. R. Unwin, *Langmuir*, **31**(43), 11932 (2015).
37. P. S. Singh, E. Kätelhön, K. Mathwig, B. Wolfrum, and S. G. Lemay, *ACS Nano*, **6**(11), 9662 (2012).
38. J. Dostál, *Operational Amplifiers*, p. 398, Butterworth-Heinemann, Stoneham, MA (1993).
39. D. A. Robinson, J. J. Yoo, A. D. Castañeda, B. Gu, R. Dasari, R. M. Crooks, and K. J. Stevenson, *ACS Nano*, **9**(7), 7583 (2015).